

Are GRBs the same at high and low redshift?

OWEN LITTLEJOHNS^{1,2}, NIAL TANVIR², RICHARD WILLINGALE², PAUL
O'BRIEN², PHIL EVANS², ANDREW LEVAN³¹*School of Earth and Space Exploration Arizona State University, Tempe, AZ
85281, USA*²*Department of Physics and Astronomy, University of Leicester, University Road,
Leicester, LE1 7RH, UK*³*Department of Physics, University of Warwick, Coventry, CV4 7AL, UK*

Due to their highly luminous nature, gamma-ray bursts (GRBs) are useful tools in studying the early Universe (up to $z = 10$). We consider whether the available subset of *Swift* high redshift GRBs are unusual when compared to analogous simulations of a bright low redshift sample. By simulating data from the Burst Alert Telescope (BAT; Barthelmy et al. 2005) the light curves of these bright bursts are obtained over an extensive range of redshifts, revealing complicated evolution in properties of the prompt emission such as T_{90} .

PRESENTED AT

GRB 2013

the Seventh Huntsville Gamma-Ray Burst Symposium
Nashville, Tennessee, 14–18 April 2013

1 Introduction

An important question in the field of GRBs is whether their populations change with redshift. This, in principle, might be reflected in the typical prompt behaviour. Beyond the dearth of higher redshift short ($T_{90} < 2$ s) bursts, the only tentative evidence for an evolution in the population of long-GRBs is that a majority (6/7) of the highest redshift ($z > 6$) GRBs found to-date have apparently rather short durations, $T_{90}/(1+z) < 5$ s (see Figures 1 & 2). Such values are of particular interest as they approach the classical value of 2 seconds used as a crude estimate of whether a burst is long or short (Kouveliotou et al. 1993, although see also Bromberg et al. 2013).

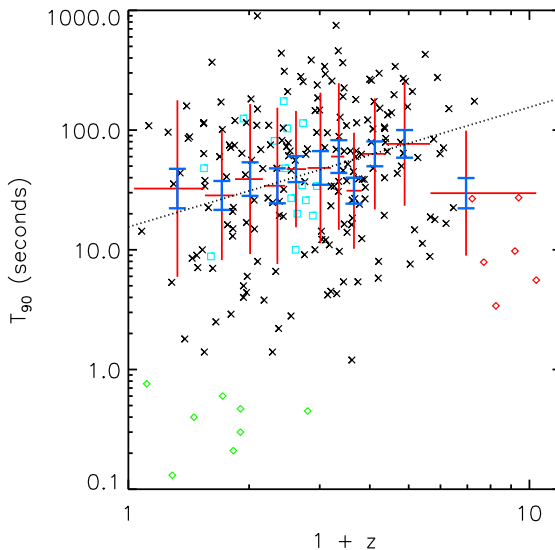


Figure 1: The observed distribution of T_{90} for the 203 *Swift* (Gehrels et al., 2004) bursts with a redshift estimate prior to the 15th of July 2012. Also included are GRB 120521C and GRB 120923A which are both candidates for high redshift. The red crosses show geometric averages of bursts taken with 20 bursts in each bin (except in the final bin which has 16 bursts). The red error bars shown in the vertical direction show the root mean square (RMS) scatter calculated logarithmically. Also shown are the standard errors on the mean for each bin in blue. The dotted black line shows the expected evolution due to simple cosmological time dilation, namely $T_{90} \propto 1+z$. Short GRBs are denoted by the green diamonds. The high-redshift subset of 6 GRBs shown in Figure 2 are indicated by red diamonds.

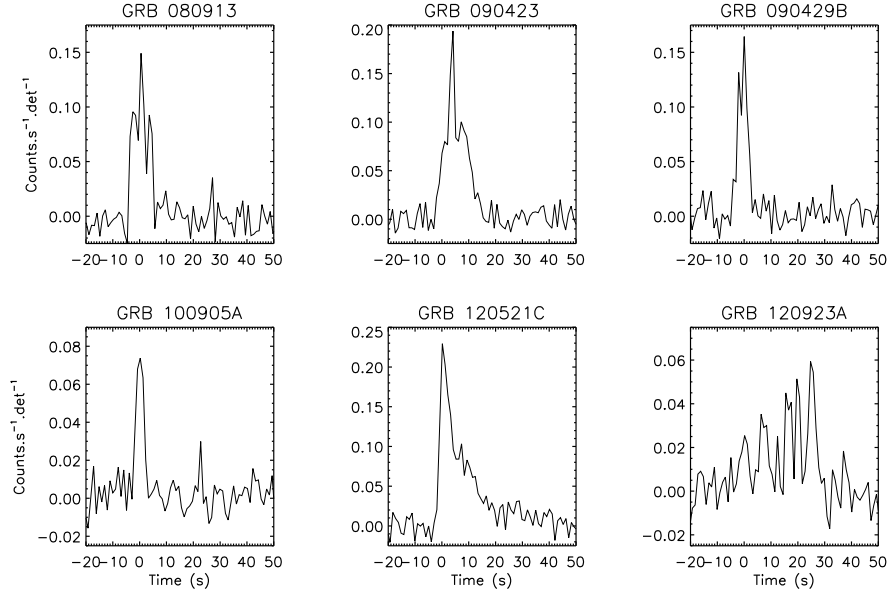


Figure 2: 15–350 keV light curves of rate-triggered GRBs within the high-redshift subset. The light curves are binned at 1024 ms to allow clearer identification of the structure within each.

2 Method

The creation of the simulated light curves required accounting for the effects of cosmological time dilation; of band shifting, as individual photons are redshifted (this included consideration of the BAT response and change in background as a function of energy); and of declining flux due to increased luminosity distance.

We used model fits obtained using the methodology with which Willingale et al. (2010) applied the pulse model of Genet & Granot (2009). The characteristic times, energies and normalising fluxes for each pulse were calculated at the simulated redshift using Equations 1 to 3.

$$T_{\text{sim}} = \left(\frac{1 + z_{\text{sim}}}{1 + z_{\text{orig}}} \right) T_{\text{orig}}, \quad (1)$$

$$E_{\text{pk,sim}} = \left(\frac{1 + z_{\text{orig}}}{1 + z_{\text{sim}}} \right) E_{\text{pk,orig}}, \quad (2)$$

$$S_{\text{pk,sim}} = \left(\frac{K_{\text{orig}}}{K_{\text{sim}}} \right) \left(\frac{D_{\text{L,orig}}}{D_{\text{L,sim}}} \right)^2 S_{\text{pk,orig}}, \quad (3)$$

where T denotes a characteristic time, z is redshift, E_{pk} is the peak energy of each pulse spectrum, S_{pk} is the normalising flux, K is the k-correction and D_{L} is the luminosity distance.

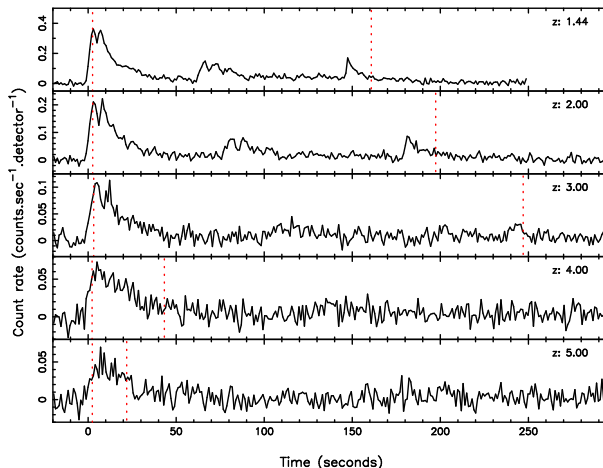


Figure 3: Simulated 15–350 keV light curves of GRB 100814A ($z_{\text{orig}} = 1.44$) at a variety of redshifts. The binning of these light curves is 1024 ms, and the red dotted line shows the start and end of the identified T_{90} period. Note that the vertical scale of each panel is independent to allow structure to be seen in all panels.

Noise was added to the light curves, before using a rate-triggering algorithm designed to establish whether BAT would trigger on the observed flux. Those bursts which were bright enough to create a trigger were then run through the standard BATTBLOCKS software to obtain T_{90} .

3 Results

Example simulated light curves for GRB 100814A are shown in Figure 3. The top three panels show an increase in measured T_{90} with redshift. At higher redshifts late-time structure is no longer detectable, thus T_{90} reduces.

Unlike previous work (Kocevski & Petrosian, 2013) the simulated GRBs contained multiple pulses. As such three effects were apparent in the $T_{90}(z)$ evolution: the time dilation of pulses and intervening quiescent periods, the gradual loss of the emission “tail” of individual pulses and the total loss of fainter (often late-time) pulses.

Figure 4 shows the impact of these competing effects on duration and also provides a good comparison between the observed high-redshift sample and simulations of the bright low-redshift bursts. Even taking the 16 bursts with the brightest features at low-redshifts, only approximately half of these remain detected at $z > 6$. This confirms that the detected high-redshift bursts only represent the luminous tail of the total population.

The observed high-redshift sample contains four bursts in the $5 < T_{90} < 10$ s regime and now also two with $T_{90} \sim 30$ s. For those simulated bursts which are still

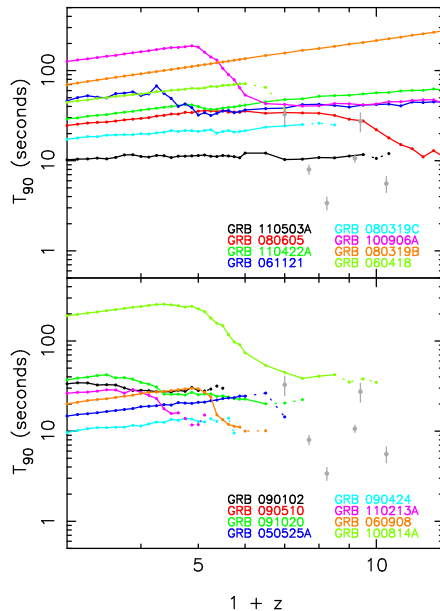


Figure 4: The evolution of T_{90} (averaged over 100 simulations per burst) as a function of redshift. The sample has been split according to the luminosity of the brightest pulse in each burst, with the most luminous 8 being shown in the top panel. Solid lines show where the bursts was detected in a minimum of 90% of the repeated simulations, the dotted lines show where the burst was detected in less than 90% but greater than 50% of these repeats. Each burst is represented by a different colour data set. The grey points correspond to the 15–350 keV T_{90} values of the observed high redshift bursts.

visible at $z > 6$, the typical duration is $30 < T_{90} < 70$ s. This suggests the two populations are different, although the analysis is limited by a small sample size.

4 Conclusions

Predicting the evolution of T_{90} with redshift is complicated. It is a combination of cosmological time dilation of structure and intervening quiescence, gradual loss of the pulse “tails” and the total loss of fainter structure.

Simulating bright low-redshift bursts at high redshifts show that only the very brightest structure is detected. While the two most recent high-redshift candidates are longer in duration, the simulations typically have longer T_{90} values.

Using the simulation technique developed with more GRBs detected at high-redshift will allow us to fully answer whether GRBs are the same at high-redshift.

ACKNOWLEDGEMENTS

This work is supported at the University of Leicester by the STFC.

References

Barthelmy S. D., et al., 2005, *Space Sci. Rev.*, 120, 143

Bromberg O., Nakar E., Piran T., Sari R., 2013, *ApJ*, 764, 179

Gehrels N., et al., 2004, *ApJ*, 611, 1005

Genet F., Granot J., 2009, *MNRAS*, 399, 1328

Kocevski D., Petrosian V., 2013, *ApJ*, 765, 116

Kouveliotou C., Meegan C. A., Fishman G. J., Bhat N. P., Briggs M. S., Koshut
T. M., Paciesas W. S., Pendleton G. N., 1993, *ApJL*, 413, L101

Willingale R., Genet F., Granot J., O'Brien P. T., 2010, *MNRAS*, 403, 1296